Fluence-dependent formation of Zn and ZnO nanoparticles by ion implantation and thermal oxidation: An attempt to control nanoparticle size

H. Amekura, M. Ohnuma, N. Kishimoto, Ch. Buchal, and S. Mantl

Citation: Journal of Applied Physics **104**, 114309 (2008);
View online: https://doi.org/10.1063/1.3014032
View Table of Contents: http://aip.scitation.org/toc/jap/104/11
Published by the American Institute of Physics

Articles you may be interested in

Embedment of ZnO nanoparticles in SiO_2 by ion implantation and low-temperature oxidation
Applied Physics Letters **90**, 083102 (2007); 10.1063/1.2709509

Fluence-dependent formation of Zn and ZnO nanoparticles by ion implantation and thermal oxidation: An attempt to control nanoparticle size

H. Amekura,[1,a)] M. Ohnuma,[1] N. Kishimoto,[1] Ch. Buchal,[2] and S. Mantl[2]
[1]*National Institute for Materials Science, 3-13 Sakura, Tsukuba, Ibaraki 305-0003, Japan*
[2]*Institut fuer Bio-und Nanosysteme (IBN1-IT), Forschungszentrum Juelich GmbH, D-52425 Juelich, Germany*

(Received 13 June 2008; accepted 23 September 2008; published online 8 December 2008)

For possible control of the size of nanoparticles (NPs), the fluence-dependent formation of Zn and ZnO NPs by ion implantation with and without thermal oxidation was investigated by optical absorption spectroscopy, Rutherford backscattering spectrometry, and small-angle x-ray scattering (SAXS). The mean diameter and number density of Zn NPs in the as-implanted state in silica (SiO_2) were determined by SAXS as 7 nm and 13×10^{17} cm^{-3}, 12 nm and 3.8×10^{17} cm^{-3}, and 12 nm and 3.2×10^{17} cm^{-3} for fluences of 0.50, 1.0, and 2.0×10^{17} ions/cm^2, respectively. With increasing fluence, the mean diameter of the NPs increases and the number density decreases. However, an upper limit of the NP size and Zn concentration in SiO_2 is observed above the fluence of 1.0×10^{17} ions/cm^2 due to sputtering loss. Thermal annealing in oxygen gas at 700 °C for 1 h induces the transformation of Zn NPs to both ZnO NPs and the Zn_2SiO_4 phase. With decreasing fluence, the branching ratio to the ZnO component decreases. This is because the reaction between tentatively formed ZnO NPs and the SiO_2 substrate is enhanced by the higher surface-to-volume ratio of smaller NPs. At a fluence of 0.20×10^{17} ions/cm^2, almost no ZnO component was detected. The size control of Zn and ZnO NPs is therefore possible only in a limited fluence region. © *2008 American Institute of Physics*. [DOI: 10.1063/1.3014032]

I. INTRODUCTION

Zinc oxide (ZnO) has been attracting considerable attention as a wide-gap semiconductor with a large exciton binding energy.[1] The concentrated oscillator strength of the exciton transition can be utilized even at room temperature (RT) and laser action is readily attainable even in nanostructures.[2,3] Furthermore, new lasing phenomena such as the random laser[2] and self-formed cavity laser[3] have been observed. Nanostructures of ZnO are highly attractive for light-emitting and laser applications, and various attempts have been made to fabricate ZnO nanostructures of high quality.

One of the successful processes in this field is the ion implantation and thermal oxidation (IITO) method.[4–6] Ion implantation is a nonthermal equilibrium synthesis method applicable to substantially any combination of ion species and target materials with well-controlled concentration, spatial position, and depth. It is also known as a high-purity process working in a high or ultrahigh vacuum. Ion implantation has now become established as one of the most important processes in current Si microelectronics technology. In the IITO method, Zn metal nanoparticles (NPs) are formed in transparent insulators such as silicon dioxide (SiO_2) by Zn ion implantation at several tens to a few hundred keV. The implanted samples are then annealed in an oxidizing atmosphere so that the Zn NPs are oxidized to ZnO NPs.[4,6]

Up to now, we have fabricated ZnO NPs of high quality under certain fabrication conditions, producing NPs that exhibit defect-band-free photoluminescence (PL).[7] However, we have not observed large blueshifts of the exciton PL under the fabrication parameters that we have examined. This is because the sizes of the NPs have always been larger than ~10 nm.[7] An attempt to control the size of NPs is described in this paper. The strategy adopted was a simple one based on the mass conservation law. Specifically, if the ion fluence decreases (increases), the size of NPs and/or the number density of NPs should decrease (increase) due to the mass conservation law. Needless to say, excessive reduction in the fluence below the solubility limit hinders the formation of NPs, while the solubility limit of Zn atoms in SiO_2 has not been determined. In the first half of this paper, the fluence dependences of the size and depth distributions of Zn metal NPs in the as-implanted state are described. In the latter half, the fluence-dependent transformation of Zn NPs to ZnO NPs by thermal oxidation is described.

II. EXPERIMENTAL

Optical-grade silica glass (SiO_2) discs of the KU-1 type (OH^- ~ 820 ppm), 15 mm in diameter and 0.5 mm in thickness, were implanted with $^{64}Zn^+$ ions of 60 keV. Samples with four different fluences of 0.20, 0.50, 1.0, and 2.0×10^{17} ions/cm^2 were prepared. Hereafter, these are referred to by the sample codes of 2E16, 5E16, 1E17, and 2E17, respectively, as listed in Table I. The ion flux was limited to less than 2 $\mu A/cm^2$ in order to maintain the sample temperature below 100 °C during implantation. In the latter half of this paper, the effects of isochronal annealing are described. Isochronal annealing was carried out at each fluence

a)Author to whom correspondence should be addressed. Electronic mail: amekura.hiroshi@nims.go.jp. FAX: +81-29-863-5599. Tel.: +81-29-863-5479.

 © 2008 American Institute of Physics

TABLE I. Sample codes, fluences, and Zn atom contents of samples determined by RBS. The mean diameter (D), total number (N) of NPs, mean interparticle distance (L_{av}), and number density (n) of NPs obtained from the L_{av} values are also shown, all of which were determined in the as-implanted state by SAXS. The values in the square brackets are the relative values of the number density with the number density of sample 5E16 set as unity. ND: Below the detection limit.

Code	2E16	5E16	1E17	2E17
Fluence (10^{17} ions/cm^2)	0.20	0.50	1.0	2.0
Zn content (10^{17} ions/cm^2)	0.19 ± 0.05	0.48 ± 0.08	1.03 ± 0.10	0.82 ± 0.10
Mean diameter D_{av} (nm)	ND	7 ± 1	12 ± 2	12 ± 2
Total number of NPs N (arbitrary unit)	ND	1.0 ± 0.2	0.5 ± 0.1	0.5 ± 0.1
Mean interparticle distance L_{av} (nm)	ND	11 ± 1	17 ± 1	18 ± 1
Number density of NPs n (cm^{-3})	ND	$(13 \pm 3) \times 10^{17}$ [1.00 ± 0.21]	$(3.8 \pm 0.6) \times 10^{17}$ [0.29 ± 0.08]	$(3.2 \pm 0.5) \times 10^{17}$ [0.24 ± 0.06]

in flowing oxygen gas at a pressure of ~1 atm in a tube furnace at temperatures of 200, 400, 600, 700, 800, and 900 °C for 1 h.

A dual-beam spectrometer was used for transmittance and reflectance measurements in the wavelength region of 190–1700 nm with a resolution of 1 nm at RT. Absorption spectra were obtained from the transmittance and reflectance with a correction for multiple reflections in the samples.[8] Rutherford backscattering spectrometry (RBS) was carried out to determine the depth profiles and total content of Zn atoms in the samples using a 2.06 MeV He^+ beam of 1 mm in diameter with a scattering angle of 160°. To reduce charging effects during the measurements, the samples were covered with Al foils except for the evaluation spots. The data were analyzed using the RUMP code.[9] The thickness of the sputtered layers was evaluated from the step height at the boundaries between the implanted and masked regions using a Dektak surface profiler. Small-angle x-ray scattering (SAXS) was carried out in a transmission geometry using a molybdenum $K\alpha$ x-ray source (λ_o=0.070 93 nm). The samples were irradiated by collimated monochromatic x rays, and the scattered x rays ($0.12° <$ Scattering angle $2\theta < 2.6°$) were collected by two-dimensional position-sensitive proportional counters. The samples were not subjected to any treatments such as removal or thinning of the SiO_2 substrates. The signals from the implanted samples consisted of contributions from both the Zn NPs and the SiO_2 substrate, and the latter contribution was approximated by the signal from an unimplanted SiO_2 sample and subtracted. After subtraction of the substrate contribution, the scattering intensity I showed clear $I \propto q^{-4}$ dependences of more than one order of magnitude, where q denotes the wave number

$$q = \frac{4\pi \sin\left(\frac{2\theta}{2}\right)}{\lambda_o}, \tag{1}$$

indicating sharp interfaces of NPs, i.e., these observations support the appropriateness of this subtraction procedure.

Two different ion-range simulation codes, SRIM2003 (Ref. 10) (neglecting sputtering loss and compositional changes) and TRIDYN (Ref. 11) (including sputtering loss and compositional changes), were used to simulate the depth profiles of the implanted Zn ions. The total numbers of pseudoparticles used for the simulations with the SRIM and TRIDYN codes were 100 000 and 75 000, respectively. In the TRIDYN calculation, we set that one pseudoparticle represented 4×10^{12} Zn ions/cm^2. However, the SRIM code cannot calculate fluence dependence directly but the ratio depth profile per incident ion. The fluence dependence was therefore calculated by multiplying the number of incident ions, i.e., the fluence, to the ratio profile per ion. Consequently, the shapes of the depth profiles calculated by the SRIM code are always the same except for the peak height, as shown in Fig. 4. In this case, the 100 000 pseudoparticles corresponded to the fluence, e.g., 5×10^{16} or 1×10^{17} ions/cm^2.

For fair comparison, the same parameter values were input into both codes, namely, displacement energies of 25.0, 15.0, and 28.0 eV, lattice binding energies of 3.0, 2.0, and 3.0 eV, and surface binding energies of 1.35, 4.70, and 2.00 eV, respectively, for Zn, Si, and O atoms. These values of displacement energy, lattice binding energy, and surface binding energy were selected in accordance with a list included in the SRIM2003 code.[10]

III. RESULTS AND DISCUSSION

A. Zn NPs in as-implanted state

1. Saturated fluence dependence due to sputtering loss

Figure 1 shows the absorption spectra of samples 2E16, 5E16, 1E17, and 2E17 in the as-implanted state. The lowest fluence sample, 2E16, looked transparent. No absorption was detected at the energy region lower than ~3 eV; the absorption increased with energy of ~4 eV up to ~6.5 eV. Sample 5E16 showed a weak brownish color. The absorption peak was observed at ~5.2 eV and the absorption tail extended to the near-infrared region (< ~1.5 eV) through the visible region (~1.5 to ~3 eV). Sample 1E17 was a stronger brownish color. The absorption peak moved to ~4.8 eV and the peak intensity was approximately double that of sample 5E16. The absorption in the visible region also be-

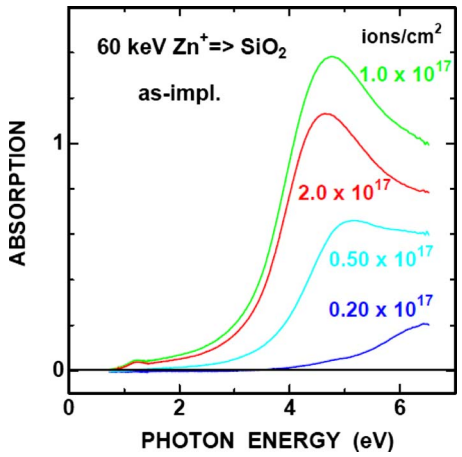

FIG. 1. (Color online) Absorption spectra of SiO_2 samples implanted with Zn^+ ions of 60 keV at fluences of 0.20, 0.50, 1.0, and 2.0×10^{17} ions/cm^2. All of the samples were evaluated in the as-implanted state.

came stronger. The highest fluence sample, 2E17, was almost the same in color as sample 1E17 as seen by the naked eye. This observation is supported by the absorption spectra: sample 2E17 shows almost the same spectrum shape as sample 1E17, while the peak energy moves slightly to ~4.7 eV and the peak intensity decreases to ~82%. It should be noted that the absorption decreases while the fluence doubles.

Similar behaviors are observed in the RBS spectra. Figure 2 shows the RBS spectra at the Zn edge (i.e., the depth profiles of Zn atoms) of the four samples whose absorption spectra were shown in Fig. 1. As the fluence increases up to 1.0×10^{17} ions/cm^2, the RBS peak linearly increases and gradually shifts to the high-energy side, i.e., the surface side. At fluences exceeding 1.0×10^{17} ions/cm^2, the peak stops increasing but shifts further toward the high-energy (surface) side.

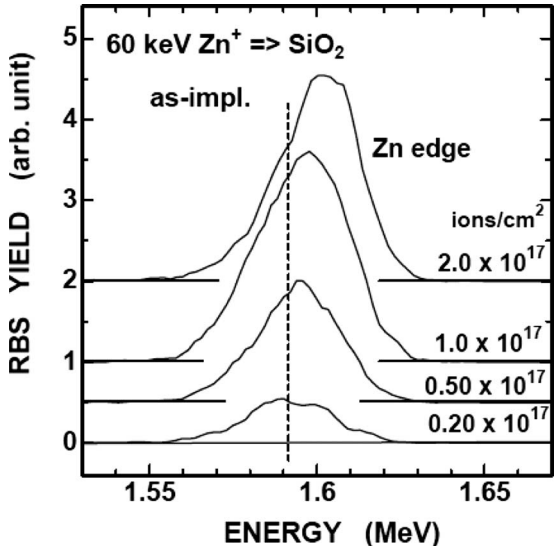

FIG. 2. RBS spectra at the Zn edge of SiO_2 samples implanted with Zn^+ ions of 60 keV at fluences of 0.20, 0.50, 1.0, and 2.0×10^{17} ions/cm^2. All of the samples were evaluated in the as-implanted state. The incident energy of the He^+ beam was 2.06 MeV. The spectra are shifted vertically for clarity and the horizontal lines indicate the base lines.

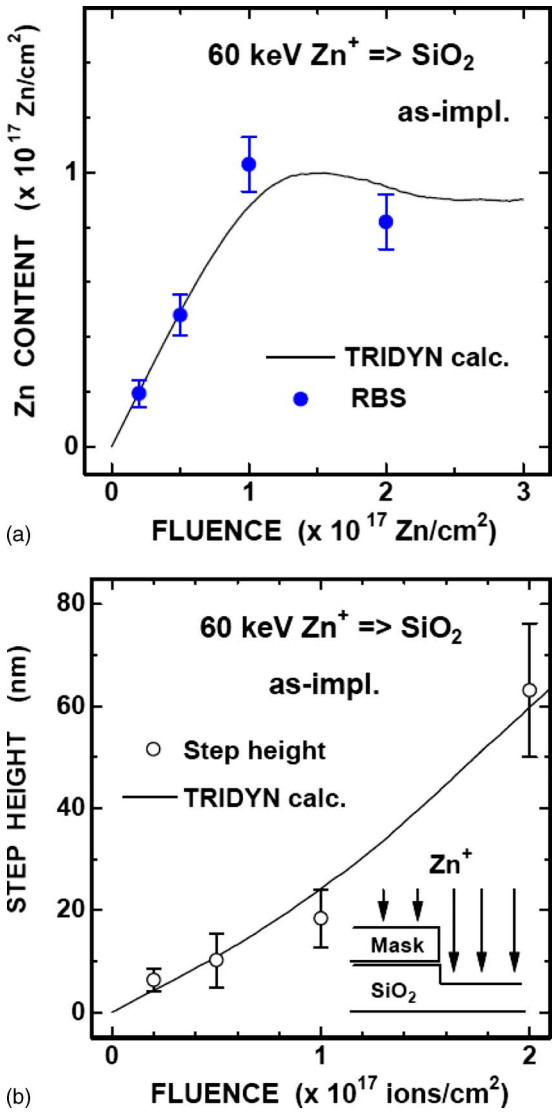

FIG. 3. (Color online) Fluence dependences of (a) the Zn content evaluated by RBS and (b) the step height of SiO_2 samples implanted with Zn^+ ions of 60 keV. All of the samples were evaluated in the as-implanted state. The step height was evaluated at boundaries between the implanted and masked regions, as illustrated in the inset in (b). The circles and lines denote experimental data and results calculated by the TRIDYN code, respectively.

The Zn content integrated along the depth, which was determined from the RBS peak at the Zn edge using the RUMP code,[9] is plotted against the fluence by closed circles in Fig. 3(a). Up to 1.0×10^{17} ions/cm^2, the Zn content linearly increases with the fluence. All of the implanted Zn atoms remain inside the substrate. When the fluence exceeds 1.0×10^{17} ions/cm^2, the Zn content shows saturation behavior. At the fluence of 2.0×10^{17} ions/cm^2, only 0.82×10^{17} atoms/cm^2 of Zn atoms, i.e., only 42% of the implanted ions, remain inside the substrate. The saturated fluence dependence of the Zn content results in the saturated fluence dependence of the absorption spectra shown in Fig. 1.

The fluence dependence of the step height at the boundaries between the implanted and the masked (unimplanted) regions is shown in Fig. 3(b) by open circles. The step formation could be ascribed to various effects such as sputtering

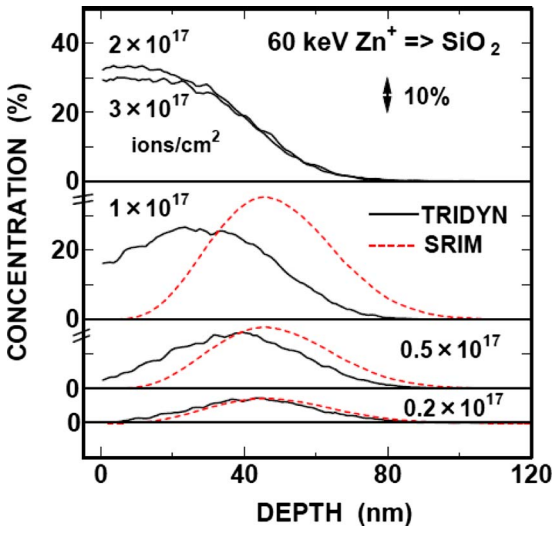

FIG. 4. (Color online) Evolution of depth profiles of Zn ions of 60 keV implanted to SiO_2 samples at various fluences calculated by TRIDYN (solid lines) and SRIM2003 (dotted lines). The profiles calculated at 2 and 3 $\times 10^{17}$ ions/cm^2 by the SRIM2003 code are not shown. The depth profiles are shifted vertically for clarity and the horizontal lines indicate the base lines.

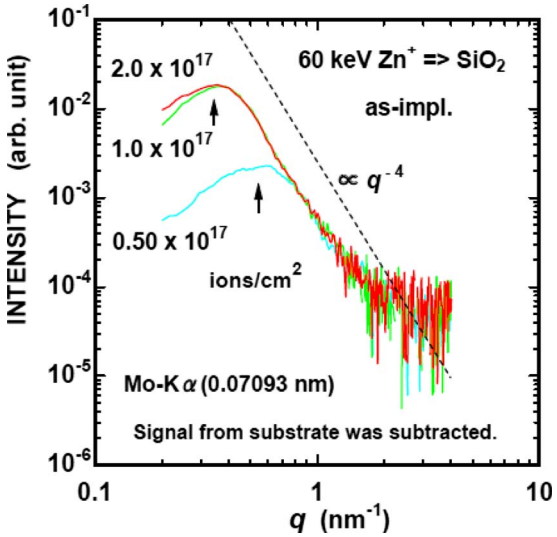

FIG. 5. (Color online) SAXS spectra of Zn NPs embedded in SiO_2 substrates, which were fabricated by implantation of Zn^+ ions of 60 keV at fluences of 0.50, 1.0, and 2.0×10^{17} ions/cm^2. The scattering contribution from the SiO_2 substrate has already been subtracted. All of the samples were evaluated in the as-implanted state.

loss in the surface layer, swelling of the surface layer due to inclusion of the implanted atoms (mass), plastic deformation of the SiO_2 substrate by ion irradiation,[12,13] etc. However, it can be seen in Fig. 3(b) that the TRIDYN calculation, which includes two effects only, i.e., the sputtering loss and the implanted mass effect, quantitatively reproduces the observed dependence of the step height. Since the sputtering loss and the implanted mass effect, respectively, decrease and increase the height of the implanted region, sputtering loss is the main mechanism forming the step in our case. It should be noted that, on the contrary, the implantation of 60 keV boron dimer ions to diamond induces a large increase in the height of the implanted region.[14] The step height increases even when the fluence exceeds 1.0×10^{17} ions/cm^2 with samples 1E17 and 2E17 showing step heights of 18.4 ± 5.7 and 63.1 ± 13.1 nm, respectively. No saturation behavior is therefore observed. Moreover, the latter height is significantly more than double the former height. This is probably due to the formation of a SiO_2 layer containing a significant number of atoms heavier than Si and O atoms, i.e., Zn atoms, beneath the surface, which reduces the ion range and enhances the sputtering. These observations again confirm that the latter sample 2E17 was implanted with double the fluence compared with the former sample 1E17.

The TRIDYN calculation provides an important insight for understanding these observations. Figure 4 shows the depth profiles of implanted Zn atoms in SiO_2 calculated by both the TRIDYN code (solid lines) and the SRIM2003 code (dotted lines). One of the main differences between TRIDYN and SRIM is that the TRIDYN code includes the sputtering loss and compositional changes due to implantation, whereas the SRIM code does not. At low fluences such as 0.2×10^{17} ions/cm^2, both codes give almost identical profiles. With increasing fluence, the TRIDYN profile moves toward the surface side due to the sputtering removal of the surface layer, while the SRIM profile always shows the identical shape but linearly increasing peak height. The shallowing of the depth profile with the fluence observed by RBS (Fig. 2) is reproduced by the TRIDYN calculation. At fluences exceeding 1.0×10^{17} ions/cm^2, TRIDYN shows saturation behavior in the depth profile while SRIM does not. The saturation of the peak height of the depth profile observed by RBS (Fig. 2) is also reproduced by the TRIDYN calculation. The TRIDYN depth profile at 1.0×10^{17} ions/cm^2 is almost the same as those at 2.0 and 3.0×10^{17} ions/cm^2. On the contrary, the SRIM code gives a maximum concentration of ~60 and ~90 at. % of Zn atoms in SiO_2 (not shown in the figure) at fluences of 2.0 and 3.0×10^{17} ions/cm^2, respectively, which is not realistically attainable. The fluence dependences of the Zn content and the step height calculated by the TRIDYN code are shown by solid lines in Figs. 3(a) and 3(b), respectively. Good agreement was obtained between the experimental and calculated results. It should be noted that such good agreement is rather surprising since we did not use any fitting parameters for the calculations.

2. SAXS analysis

Figure 5 shows the SAXS profiles of the samples implanted at three different fluences plotted against the wave number q as defined in Eq. (1). The contribution from the SiO_2 substrate was approximated by the spectrum of an unimplanted SiO_2 sample and has already been subtracted from the data plotted in the figure. The subtracted spectra of samples 5E16, 1E17, and 2E17 in the figure show clear $I\propto q^{-4}$ dependences of more than one order of magnitude, indicating sharp interfaces of NPs, i.e., these observations also support the appropriateness of the subtraction procedure. The profiles show a peak at $q=\sim0.57$, 0.37, and 0.35 nm^{-1} for samples 5E16, 1E17, and 2E17, respectively. The peaks are due to the interference of x rays scattered by neighboring NPs, indicating the existence of a definable mean interparticle distance L_{av}. It should be noted that the

peak widths are relatively narrow in the linear plot although the widths appear very broad in the log-log plot. With regard to the lowest fluence sample (2E16), since the spectrum was almost the same as that of the unimplanted sample within the range of experimental error, it is not discussed further here.

To include the interference effect between the NPs, the SAXS profiles were evaluated based on the local monodisperse hard-sphere model.[15] In this model, the SAXS profile $I(q)$ is given as

$$I(q) \propto \int_0^\infty V(R)^2 F^2(q,R) S(q,R_{\mathrm{HS}},\eta) N(R) dR, \tag{2}$$

where $V(R)$ is the volume of a sphere of radius R, $F(q,R)$ is the form factor of a sphere of radius R, and $S(q,R_{\mathrm{HS}},\eta)$ is the structure factor of the sphere system whose structure is represented by a volume fraction η and a hypothetical hard-sphere radius R_{HS}. We assume that the number density $N(R)$ of the sphere of radius R follows a log-normal distribution

$$N(R) = \frac{1}{\sqrt{2\pi}\sigma R} \exp\left[-\frac{(\ln R - \ln R_{\mathrm{av}})^2}{\sigma^2} \right]. \tag{3}$$

The SAXS profiles $I(q)$ were fitted by Eq. (2) with optimization of parameters such as the mean radius (R_{av}), the dispersion (σ), the volume fraction (η), and a hypothetical hard-sphere radius (R_{HS}). The mean interparticle distance (L_{av}) was determined directly from the peak wave number (q_{peak}) as

$$L_{\mathrm{av}} = \frac{2\pi}{q_{\mathrm{peak}}}. \tag{4}$$

It is clear from the definition that L_{av} refers to the mean distance between the centers of neighboring NPs.

The determined size distributions are shown in Fig. 6(a). The fluence dependences of the parameters, i.e., the mean diameter (D_{av}), mean interparticle distance (L_{av}), total number of NPs (N), and number density of NPs (n), are summarized in Fig. 6(b) and Table I. Since the absolute scattering cross section of a NP of any given size is known, the total number (N) of NPs is obtained by a comparison between the experimental and calculated intensities. On the other hand, the number density (n) of NPs was determined directly from the interparticle distance L_{av} using the following relation:

$$n = \left\{ \frac{4\pi}{3} \left(\frac{L_{\mathrm{av}}}{2} \right)^3 \right\}^{-1}. \tag{5}$$

Samples 5E16, 1E17, and 2E17 have mean diameters of 7 ± 1, 12 ± 2, and 12 ± 2 nm, respectively. Again the saturation is visible at the high fluences. The size distribution of sample 5E16 shows a much higher peak height in Fig. 6(a) because Fig. 6(a) plots the total *number* of NPs. Sample 5E16 contains smaller but many more NPs.

As shown in Fig. 6(b), the number density n of NPs decreases more rapidly than the total number N of NPs in the sample with increasing fluence. Since the relation $n = N/V$ holds between the number density n and total number N of NPs, where V denotes the effective volume (or thickness in the present case) of the layer where NPs are formed, the steeper decrease in the number density is ascribed to the increase in the effective thickness of the layer containing NPs. This behavior is qualitatively consistent with the prediction from the TRIDYN code shown in Fig. 4. The concentration profile along the depth becomes flatter with increasing fluence as shown in Fig. 4, i.e., the effective thickness increases.

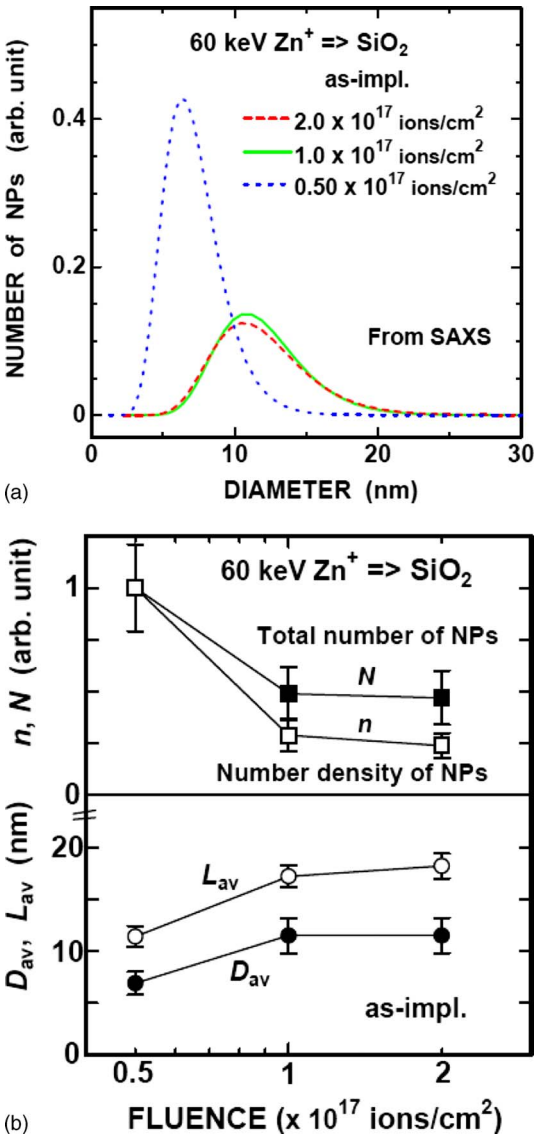

FIG. 6. (Color online) (a) Size distributions of Zn NPs determined from SAXS measurements of SiO_2 samples implanted with Zn^+ ions of 60 keV at fluences of 0.50, 1.0, and 2.0×10^{17} ions/cm^2. All of the samples were evaluated in the as-implanted state. (b) Fluence dependences of the mean diameter (D_{av}, closed circles), mean interparticle distance (L_{av}, open circles), total number of NPs (N, closed squares), and number density of NPs (n, open squares) determined from L_{av}, plotted against the fluence.

Changes in the size and number of NPs under additional ion implantation can be described by classical nucleation and growth theory under additional monomer supply. In fact, such a theory has been developed.[16–18] Rizza *et al.*[18] categorized the evolution of the radii and number of NPs against time (or fluence) in eight different regimes with combinations of [closed/open system] × [growth/Ostwald ripening (OR) regime] × [reaction-/diffusion-limited regime]. Our results showed that the mean diameter of NPs increased as the fluence increased from 5.0×10^{16} to

1.0×10^{17} ions/cm^2 while the total number of NPs decreased. Five categories, i.e., four categories of growth regime and the diffusion-limited OR of the open system, were excluded because they predict a constant number of NPs. Although the OR regimes of the closed system predict a decrease in the number of NPs with the fluence, our implantation conditions are far from those of a closed system. The most likely category is the reaction-limited OR regime of the open system. Rizza *et al.*[18] categorized gold NPs under 4 MeV Au ion irradiation as the diffusion-limited OR regime of the open system. Judging from a comparison of the thermal stability of Zn NPs and Au NPs in SiO_2,[19] the diffusion constant of Zn atoms in SiO_2 is considered to be much higher than that of Au atoms. The different regimes of Zn NPs and Au NPs under different irradiation conditions are not surprising.

However, the theory predicts power-law dependences of the radii (R) and number (N) of the NPs as

$$R \propto t^{1/2} \quad \text{and} \quad N \propto t^{-1/2} \tag{6}$$

for the reaction-limited OR regime of the open system,[18] while our experiments give dependences of

$$R \propto t^{0.78} \quad \text{and} \quad N \propto t^{-1.0}. \tag{7}$$

Agreements of the powers are rather poor. These discrepancies are probably due to the fact that our system is no longer a simple homogenous system with a constant monomer supply. As shown in Fig. 2, the Zn concentration strongly depends on the depth, and the depth profile changes with the fluence. The monomers are supplied not homogeneously along the depth but selectively around the ion range. Furthermore, the Zn NPs and atoms are lost not homogeneously along the depth but selectively from the surface by sputtering. As described above, the effective volume of the system itself changes with the fluence. It is therefore probably that the assumptions of the theory are not exactly applicable to our system.

On the contrary, samples 1E17 and 2E17 show almost the same size distribution, mean interparticle distance, and total number of NPs, indicating that these quantities are determined mainly by the concentration of Zn atoms, not the fluence. This behavior is completely different from that expected from the nucleation and growth theory with a homogenous monomer supply. As already described, the difference probably arises from the complex nature of our implantation conditions. The insensitivity of the size distribution of NPs observed above the fluence of 1×10^{17} ions/cm^2 indicates that the size control of Zn NPs in the as-implanted state by fluence is only possible in a limited fluence region.

B. Transformation to ZnO NPs by oxidation annealing

According to our previous studies[20,21] on SiO_2 samples implanted with Zn^+ ions of 60 keV to 1.0×10^{17} ions/cm^2, annealing in oxygen gas at 700 °C for 1 h induces the transformation of Zn NPs to ZnO NPs by oxidation. However, some of the formed ZnO NPs react further with the SiO_2 substrate and are transformed to the Zn_2SiO_4 phase. The branching ratio to the Zn_2SiO_4 phase (the ZnO NPs) increases (decreases) in samples annealed at 800 °C. Finally only the Zn_2SiO_4 phase forms at the annealing temperature of 900 °C.[20]

The absorption spectra of samples 2E16, 5E16, 1E17, and 2E17 were measured at RT after they were annealed in oxygen gas at various temperatures between 200 and 900 °C. Some typical results for samples 2E16, 5E16, and 1E17 are summarized in Figs. 7(a)–7(c). To ensure fair comparisons, the absorption was divided by the Zn atomic content of the samples as determined by RBS. The results obtained for sample 2E17 were similar to those for sample 1E17. This is reasonable because the size distributions of the Zn NPs and the Zn atomic content, i.e., the initial conditions before oxidation, are almost the same in these two samples.

In both of samples 5E16 and 1E17, broad absorption due to Zn NPs is observed with a peak around 4.5 to 5.0 eV in the as-implanted state. After annealing in oxygen gas at 700 °C for 1 h, the exciton peak of ZnO NPs appears at ~3.3 eV in both samples. However, the exciton peak of sample 5E16 is weaker than that of sample 1E17 although the absorption was plotted after the normalization of the Zn atomic content. In contrast, the absorption edge at ~5.4 eV, which corresponds to the Zn_2SiO_4 phase,[22] of sample 5E16 is stronger than that of sample 1E17. These findings indicate that the branching ratio to the ZnO (Zn_2SiO_4) phase of sample 5E16 is smaller (larger) than that of sample 1E17. After annealing at 900 °C, both the ZnO peaks disappear while similar intensities of the absorption edges of the Zn_2SiO_4 phase remain.

In the case of sample 2E16 in the as-implanted state, absorption started at around ~3 eV and monotonically increased up to the detection limit of ~6.5 eV. No peak was observed. After annealing at 200 °C (not shown), the spectrum was almost the same as that of the as-implanted state. After annealing at 400 °C, the spectrum shifted slightly to the low-energy side but was similar to that of the as-implanted state. After annealing at 600 °C, the spectrum was similar to that of the as-implanted state but slightly weaker in the high-energy region.

One of the surprising results obtained is that the exciton peak of ZnO NPs does not appear even after annealing at 700 °C for 1 h, which is one of the best oxidation conditions for samples implanted at higher fluences. Only the absorption edge of the Zn_2SiO_4 phase at ~5.4 eV is observed after annealing at 700 °C. This is consistent with the results shown in Figs. 7(a) and 7(b), indicating that the branching ratio to ZnO NPs decreases with decreasing fluence. After annealing at higher temperatures, i.e., 800 and 900 °C, the spectrum is similar but the magnitude of the Zn_2SiO_4 edge slightly increases.

One possible explanation for the decrease or disappearance of the ZnO exciton peak at lower fluences could be the enhanced escape of Zn atoms during oxidation annealing at around 700 °C; however, this is excluded by the results shown in Fig. 8. The Zn atomic content of all the samples was evaluated by RBS in the as-implanted state and after annealing at 700 and 900 °C. In all of the samples, the Zn atomic content maintained the same value within the range of experimental error even after annealing at 900 °C, i.e.,

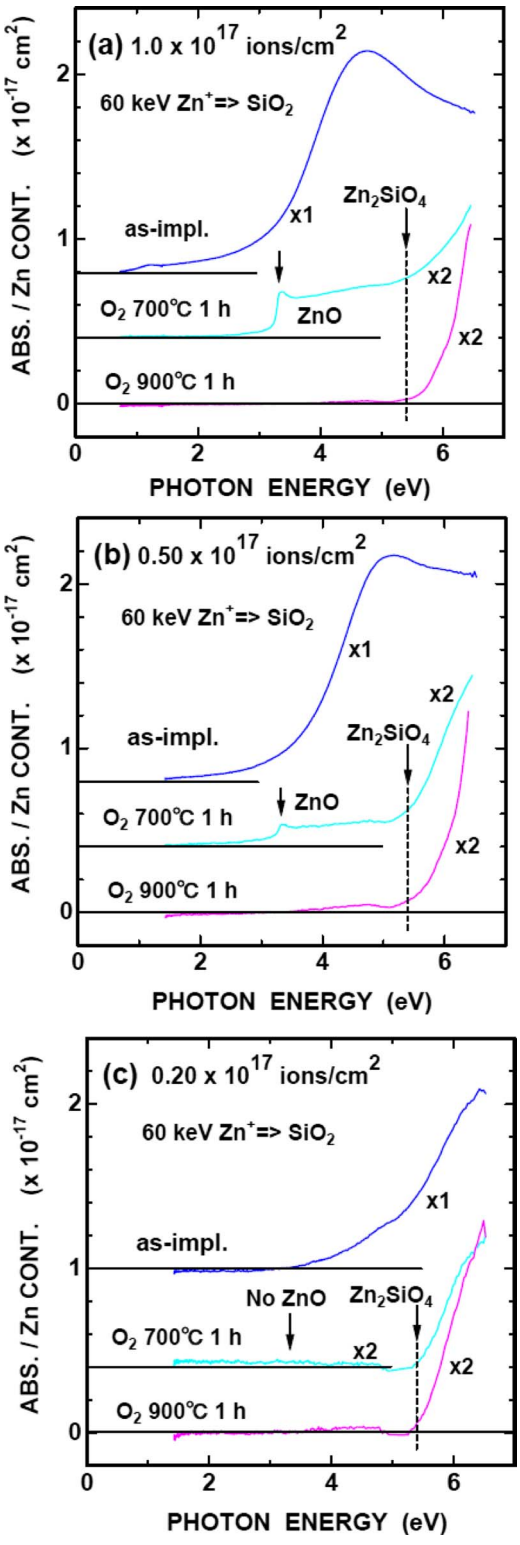

FIG. 7. (Color online) Absorption spectra normalized by the Zn atomic content of SiO_2 samples implanted with Zn^+ ions of 60 keV at fluences of (a) 1.0, (b) 0.50, and (c) 0.20×10^{17} ions/cm^2, both in the as-implanted state and after annealing in oxygen gas at 700 and 900 °C for 1 h. The peak around 3.3 eV and the absorption edge at ~5.4 eV correspond to the ZnO and Zn_2SiO_4 phases, respectively. The spectra are shifted vertically for clarity and the horizontal lines indicate the base lines.

almost none of the Zn atoms escape from the samples although the chemical states of the Zn atoms change with the annealing temperature and fluence.

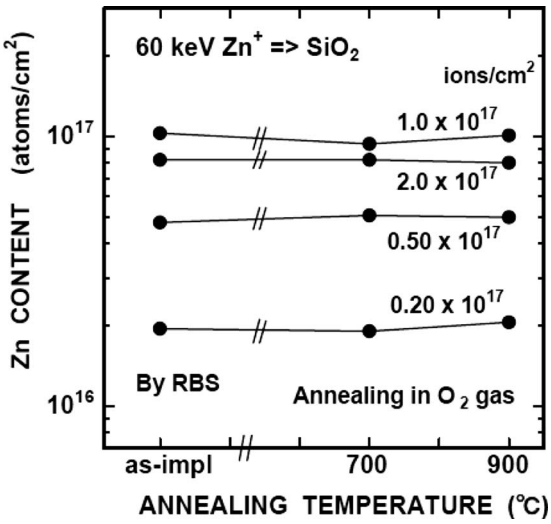

FIG. 8. Annealing temperature dependence of Zn atomic content in SiO_2 samples implanted with Zn^+ ions of 60 keV at fluences of 0.20, 0.50, 1.0, and 2.0×10^{17} ions/cm^2. Annealing was carried out in flowing oxygen gas for 1 h. It can be seen that annealing up to 900 °C does not change the Zn atomic content.

The lower (higher) branching ratio of Zn NPs to ZnO NPs (the Zn_2SiO_4 phase) at lower fluences is ascribed to the higher surface-to-volume ratio of smaller NPs. As described in Sec. III A above, lower fluence implantation generates smaller Zn NPs. Even after transportation to the surface region and transformation to ZnO NPs, the average sizes are smaller. Since the reaction rate with the SiO_2 substrate is higher for smaller ZnO NPs due to the higher surface-to-volume ratio, the branching ratio to ZnO NPs is smaller for smaller Zn NPs, i.e., at lower fluences.

IV. CONCLUSIONS

The fluence dependence of the size and depth distributions of Zn NPs, which were fabricated in SiO_2 by implantation of Zn^+ ions of 60 keV, was investigated in the as-implanted state by SAXS, RBS, optical absorption spectroscopy, step-height measurements, and TRIDYN calculation. The SAXS measurements showed that Zn NPs with mean diameters of 7, 12, and 12 nm were formed in the as-implanted state at fluences of 0.5, 1.0, and 2.0×10^{17} ions/cm^2, respectively. At fluences exceeding 1.0×10^{17} ions/cm^2, the Zn atomic content of the samples showed saturation behavior due to sputtering loss, which induces saturation of the mean diameter. Saturation due to sputtering loss was also confirmed by the absorption spectroscopy, RBS, and step-height measurements. These findings indicate that the size control of Zn NPs in the as-implanted state by fluence is possible only in a limited fluence region.

After annealing in oxygen gas at 700 °C for 1 h, the Zn NPs in SiO_2 transform to ZnO NPs or the Zn_2SiO_4 phase, irrespective of the fluence. However, the branching ratio depends on the fluence. With decreasing fluence, the branching ratio to ZnO NPs (the Zn_2SiO_4 phase) decreases (increases). This is explained by the reaction between the tentatively formed ZnO NPs and the SiO_2 substrate. The larger surface-

to-volume ratio of the smaller tentatively formed ZnO NPs enhances the reaction with the SiO_2 matrix and transformation to the Zn_2SiO_4 phase. This reaction is also an obstacle to the size control of ZnO NPs.

ACKNOWLEDGMENTS

A part of this study was supported by the Budget for Nuclear Research of the Ministry of Education, Culture, Sports, Science and Technology (MEXT) of Japan based on screening and counseling by the Atomic Energy Commission and also by the Nippon Sheet Glass Foundation for Materials Science and Engineering.

[1]U. Ozgur, Y. I. Alivov, C. Liu, A. Teke, M. A. Reschikov, S. Dogan, V. Avrutin, S.-J. Cho, and H. Morkoc, J. Appl. Phys. **98**, 041301 (2005).
[2]H. Cao, Y. G. Zhao, S. T. Ho, E. W. Seelig, Q. H. Wang, and R. P. H. Cheng, Phys. Rev. Lett. **82**, 2278 (1999).
[3]M. Kawasaki, A. Ohtomo, I. Ohkubo, H. Koinuma, Z. K. Tang, P. Yu, G. K. L. Wong, B. P. Zhang, and Y. Segawa, Mater. Sci. Eng., B **56**, 239 (1998).
[4]Y. X. Liu, Y. C. Liu, D. Z. Shen, G. Z. Zhong, X. W. Fan, X. G. Kong, R. Mu, and D. O. Henderson, J. Cryst. Growth **240**, 152 (2002).
[5]H. Amekura, Y. Takeda, K. Kono, H. Kitazawa, and N. Kishimoto, Rev. Adv. Mater. Sci. **5**, 178 (2003).
[6]H. Amekura, N. Umeda, Y. Sakuma, N. Kishimoto, and Ch. Buchal, Appl. Phys. Lett. **87**, 013109 (2005).
[7]H. Amekura, N. Umeda, Y. Sakuma, O. A. Plaksin, Y. Takeda, N. Kishimoto, and Ch. Buchal, Appl. Phys. Lett. **88**, 153119 (2006).
[8]H. Amekura, Y. Takeda, and N. Kishimoto, Nucl. Instrum. Methods Phys. Res. B **222**, 96 (2004).
[9]L. R. Doolittle, Nucl. Instrum. Methods Phys. Res. B **15**, 227 (1986).
[10]J. F. Ziegler, J. P. Biersack, and U. Littmark, *The Stopping and Range of Ions in Solids* (Pergamon, New York, 1985).
[11]W. Möller and W. Eckstein, Nucl. Instrum. Methods Phys. Res. B **2**, 814 (1984).
[12]E. Snoeks, T. Weber, A. Cacciato, and A. Polman, J. Appl. Phys. **78**, 4723 (1995).
[13]T. van Dillen, A. Polman, C. M. van Kats, and A. van Blaaderen, Appl. Phys. Lett. **83**, 4315 (2003).
[14]H. Amekura and N. Kishimoto, J. Appl. Phys. **104**, 063509 (2008).
[15]J. S. Pedersen, J. Appl. Crystallogr. **27**, 595 (1994).
[16]E. Brosh and A. Kiv, J. Nucl. Mater. **306**, 173 (2002).
[17]K. Nozawa, M.-H. Delville, H. Ushiki, P. Panizza, and J.-P. Delville, Phys. Rev. E **72**, 011404 (2005).
[18]G. Rizza, Y. Ramjauny, T. Gacoin, L. Vieille, and S. Henry, Phys. Rev. B **76**, 245414 (2007).
[19]H. Amekura (unpublished).
[20]H. Amekura, K. Kono, N. Kishimoto, and Ch. Buchal, Nucl. Instrum. Methods Phys. Res. B **242**, 96 (2006).
[21]H. Amekura, N. Umeda, M. Yoshitake, K. Kono, N. Kishimoto, and Ch. Buchal, J. Cryst. Growth **287**, 2 (2006).
[22]H. Chang, H. D. Park, K. S. Sohn, and J. D. Lee, J. Korean Phys. Soc. **34**, 545 (1999).